Journal of Materials Research and Technology 27 (2023) 4012–4022

Contents lists available at ScienceDirect

Journal of Materials Research and Technology

journal homepage: www.elsevier.com/locate/jmrt

Recycled glass powder for enhanced sustainability of limestone calcined clay cement (LC3) mixtures: mechanical properties, hydration, and microstructural analysis

Yi-Sheng Wang [a], Seokhoon Oh [a], Shafiq Ishak [b], Xiao-Yong Wang [a,c,*], Seungmin Lim [d,**]

[a] Department of Integrated Energy and Infra System, Kangwon National University, Chuncheon-si, 24341, Republic of Korea
[b] Department of Structure and Materials, Faculty of Civil Engineering, University of Technology Malaysia (UTM), Johor Bahru, 81310, Johor, Malaysia
[c] Department of Architectural Engineering, Kangwon National University, Chuncheon-si, 24341, Republic of Korea
[d] Department of Architecture, Kangwon National University, Chuncheon 24341, Republic of Korea

ARTICLE INFO

Handling Editor: Prof. M Meyers

Keywords:
Hydration
Limestone calcined clay cement (LC^3)
Recycled glass powder
Supplementary cementitious material (SCM)
Sustainable

ABSTRACT

The large quantities of nondegradable waste glass led to landfill overflow, causing severe environmental harm. Measures need to be taken to reduce the environmental problems associated with waste glass. Limestone calcined clay cement (LC^3) has excellent performance and a low-carbon footprint. However, its environmental benefits still require improvement. This study proposes a strategy to partially replace LC^3 with recycled glass powder (RGP) to utilize waste glass while reducing CO_2 emissions further. RGP replacement percentages are 10 and 20 %. Experimental studies were systematically conducted to investigate the performance, product composition, and CO_2 emission of RGP-LC^3. Experimental tests on a macro scale include workability, mechanical properties, and ultrasonic pulse velocity. The composition and microstructure of the material were characterized using thermogravimetric, Fourier-transform infrared, X-ray diffraction, and scanning electron microscopy. The CO_2 emissions of LC^3 at different stages of its lifecycle were compared and discussed how RGP can reduce these emissions. The results show that RGP helps to increase the workability of the slurry. LC^3 containing 10 % RGP showed similar compressive strength to the control group, and 20 % RGP resulted in a decrease in strength. As the replacement percentages increase from 0 to 10 and 20 %, the CO_2 emissions per unit volume decrease from 606.46 to 545.14 and 484.43 kg m^3/MPa.

1. Introduction

Waste glass accounts for 5 % of global waste, and approximately 130 million tons of waste glass products are generated annually [1]. However, owing to its nondegradable properties, 75 % of waste glass is landfilled. This results in landfill overflow and requires measures to mitigate its environmental hazards. Recycled glass powder (RGP) is a powder material with an appropriate particle size that can be ground from waste glass. Carsana et al. showed that the pozzolanic activity of the RGP is sustained for up to seven years [2], and the activity increased as the particle size decreased [3,4]. Low-carbon and low-cost RGP can be applied as a supplementary cementitious material (SCM) in construction projects, providing significant ecological and economic benefits in terms of CO_2 emissions, energy consumption, and economic costs [5,6]. Moreover, by promoting the application of RGP in the construction field, it can also reduce the space pressure of landfills and effectively reduce the negative impact of waste glass on the environment.

Limestone calcined clay cement (LC^3) is a high performance composite material with a low-carbon footprint [7–9], and is capable of reducing CO_2 emissions by 30–40 % per ton compared to traditional cement [10]. LC^3 is currently being implemented in an increasing number of countries and regions, and is expected to occupy the largest cement market share as a substitute for OPC in the near future. LC^3 contains calcined clay and metakaolin, whose alumina and silica react with the clinker to form hydration products, improving the mechanical properties and durability of cement. Recent studies report techniques to improve the performance of LC^3 systems, such as the use of nanomaterials [11], fiber [12], and CSH seedings [13]. However, producing

* Corresponding author. Department of Integrated Energy and Infra System, Kangwon National University, Chuncheon-si, 24341, Republic of Korea.
** Corresponding author.
E-mail addresses: wxbrave@kangwon.ac.kr (X.-Y. Wang), smlim@kangwon.ac.kr (S. Lim).

https://doi.org/10.1016/j.jmrt.2023.10.245
Received 23 August 2023; Accepted 24 October 2023
Available online 4 November 2023

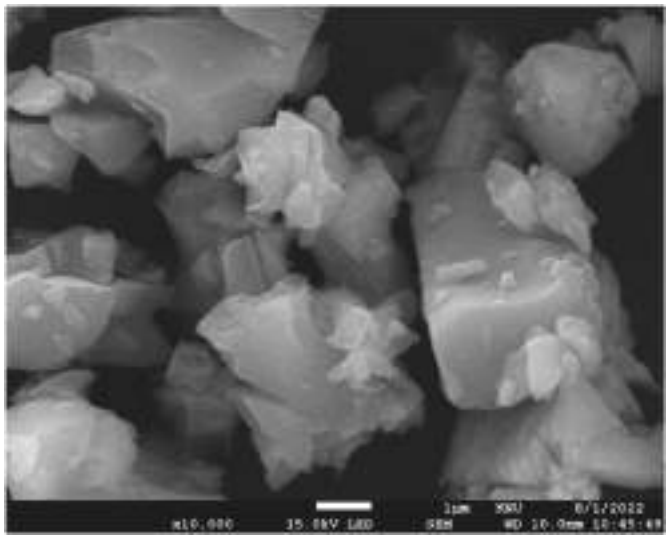

Fig. 1. SEM microscopic images of the RGP.

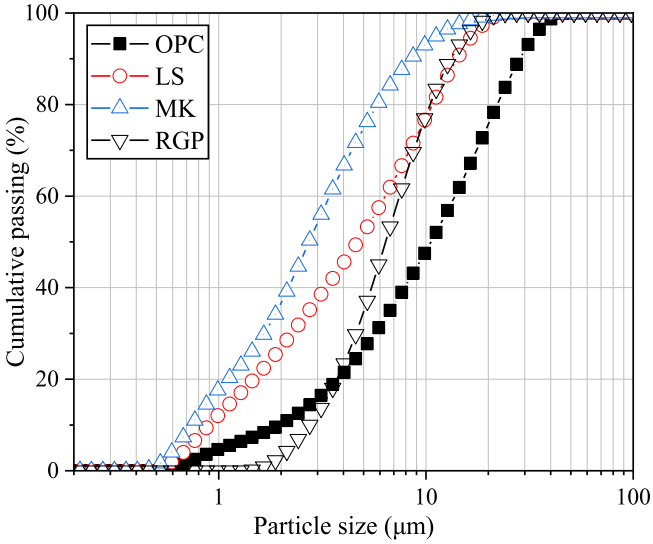

Fig. 2. Particle size distribution of OPC LS MK, and RGP.

calcined clay requires a calcination process that involves heating the clay to a high temperature of 750 °C [8]. This process also leads to greenhouse gas emissions [14]. To achieve carbon neutrality by 2050, the cement industry must undergo deep decarbonization. Therefore, improving the environmental benefits of LC^3 is crucial. This, however, requires continuous innovation and improvement. Combining low-carbon emission RGP with LC^3 would be a practical approach.

However, there are still some gaps in current research: (1) most existing conclusions are based on OPC tests, which are unsuitable for composite cement. LC^3 has a low clinker proportion and contains clay or metakaolin with high pozzolanic activity, causing the hydration and microstructure of LC^3 to differ significantly from those of OPC. (2) Previous studies have focused on a single property, such as strength development, durability, and reactivity [3,15–17]. A systematic and comprehensive analysis is still lacking to help understand the effects of RGP on the physicochemical properties of LC^3. Furthermore, it is necessary to verify whether the workability and strength of RGP-LC^3 satisfy engineering needs through experiments. (3) Most previous studies analyzed CO_2 emissions based on the 28 d compressive strength [6,18,19]. However, for the composite cement, the reactivity of some SCMs was extremely low after 28 d making CO_2 emission analysis unreasonable. Carbon emissions should be analyzed based on longer age to ensure pozzolanic reactions function.

To address the deficiencies of existing studies, this study used RGP to partially replace LC^3 at ratios of 0, 10, and 20 %, denoted as RGP-LC^3. The exothermic process was monitored by isothermal calorimetry, and the workability was tested. Mechanical properties were verified using a combined compressive strength test and ultrasonic pulse velocity (UPV) test. Changes at the microscopic level were analyzed using techniques such as thermogravimetric (TG), X-ray diffraction (XRD), Fourier-transform infrared (FT-IR), and scanning electron microscopy (SEM). Furthermore, the CO_2 emissions of RGP-LC^3 were evaluated based on the 28 d and 90 d strengths, and the positive effect of the combination of LC^3 and RGP on environmental improvement was discussed.

2. Material design and experimental details

2.1. Materials

The type I cement (OPC) was produced by the Sung Shin Cement Company and had an average particle size of 12.98 μm. Limestone (LS) with an average particle size of 4.41 μm was purchased from Daejung Chemical Co., Ltd. Metakaolin (MK) was provided by Anpeak Specialty Minerals Co., Ltd, and had an average particle size of 3.2 μm. FU HUA Mineral Co., Ltd. provided the RGP used in this study having an average particle size of 7.26 μm. As shown in Fig. 1, SEM analysis shows that RGP has a smooth morphology. Smooth surfaces often help reduce friction between particles of cementitious materials, thereby improving flowability. RGP was also observed to have a dense micromorphology, indicating the stability of its structure. Fig. 2 shows the particle size distributions of the raw materials detected using a laser particle size tester. Table 1 lists the chemical compositions of OPC LS MK, and RGP analyzed using XRF.

2.2. Mixture preparation

LC^3 in this study was made according to the LC^3-55 recommended by Scrivener et al. [7], consisting of 55 % OPC, 15 % LS, and 30 % MK. The mass of total LC^3 was partially replaced with RGP at two different percentages (10 and 20 %). The detailed design of the mixture ratios is listed in Table 2. A water/binder ratio of 0.6 was used for the preparation of all samples. The mixture slurries were prepared and cured according to the parameters listed in Table 2 to evaluate their engineering properties. The samples prepared for SEM, TGA, XRD, and FTIR analysis are newly cast for microstructure purposes. Samples were sealed in plastic vials until the age of testing.

The cement slurry was prepared using the following procedure: First, the weighed raw materials were placed into the mixer and dry mixed for 60 s to ensure even distribution. The weighed liquid was then injected into a mixer and mixed at 60 rpm for 120 s. The residual slurry was scraped off from the inner wall and bottom of the mixer and stirred for 120 s at a stirring speed of 120 rpm.

2.3. Experimental

2.3.1. Isothermal calorimetry

The heat released from the fresh cement slurry was monitored using a multichannel isothermal calorimeter (TA Instruments, USA). Approximately 5g of powder and water were added to a glass amine bottle, mixed quickly, and then sealed in an ampoule. The sealed ampoules were placed in an isothermal calorimeter for 168 h at a temperature of 20 ± 0.2 °C.

2.3.2. Workability test

To characterize the workability of the slurry, a mini-slump test was conducted following the ASTM C1437 standard. The fresh slurry was

Table 1
Chemical compositions of OPC LS MK, and RGP.

Oxide (%)	Al_2O_3	MgO	CaO	SiO_2	SO_3	Na_2O	K_2O	Fe_2O_3	LOI.
OPC	5.18	2.32	64.15	20.89	2.26	0.06	0.97	2.58	1.62
LS	0.32	1.57	54.35	1.64	–	0.05	–	–	42.09
MK	45.66	–	0.35	52.32	–	–	0.08	0.25	1.35
RGP	0.13	3.43	9.58	72.2	0.26	12.9	0.32	0.11	1.19

Table 2
Mixture proportions of the mixture (wt %).

Mix	Unit Mass				
	RGP	OPC	LS	MK	w/b
R0	0	55	15	30	0.6
R10	10	49.5	13.5	27	0.6
R20	20	44	12	24	0.6

stirred and placed in a round mold. The mold was lifted, allowing the slurry to flow. Once the slurry stopped flowing, the diffusion diameter was measured in two perpendicular directions and the average value was recorded.

2.3.3. Mechanical properties test

The mechanical properties were tested on days 3, 7, 28, 56, and 90 d of sealing curing. The compressive strengths of the cubic samples were measured according to the ASTM C109 standard. The size of the cubic sample was 50 mm × 50 mm × 50 mm. Each group was tested three times and the average value was recorded to ensure reliability.

2.3.4. UPV test

The UPV change in LC^3 was measured using a nondestructive digital tester (Pundit Lab, Procq Company, Switzerland) following the AASHTO T 358 standard. The UPV test sample was a cuboid with dimensions of 40 mm × 40 mm × 160 mm.

2.3.5. XRD analysis

Samples for XRD, TGA, and FTIR analysis were prepared at 3 and 90 d of curing, respectively. Hydration of the hardened cement paste must be stopped before compositional analysis is performed. The samples were finely ground into a powder, and hydration was stopped using the solvent exchange method [20]. Use isopropyl alcohol as the solvent to stop hydration. The filtered powder was placed in a vacuum box to remove the excess isopropanol.

The diffraction of crystals was determined using a diffractometer model PANalytical X'Pert Pro MPD (The Netherland), by XRD technique at a scan rate of 0.05° 2θ/s, scanning in the range of 5–45° 2θ.

2.3.6. TG analysis

Approximately 20 mg of powder was heated from room temperature to 1000 °C at a heating rate of 15 °C/min under nitrogen purge using a Thermogravimetric analyzer (SDT Q600, TA Instruments, USA) with a synchronized DSC system.

2.3.7. FTIR analysis

The change in the functional group absorption band in the 500–4000 cm^{-1} band of the powder sample was detected using a Nicolet iN10 FT-IR spectrometer (Thermo Scientific, Germany). Each sample was scanned 32 times.

2.3.8. SEM analysis

The hardened cement paste was crushed, and flake-like fragments were immediately used for SEM observation. A JSM-7900 F thermal field-emission scanning electron microscope (JEOL Ltd., Japan) was used for energy-dispersive X-ray spectroscopy (EDS).

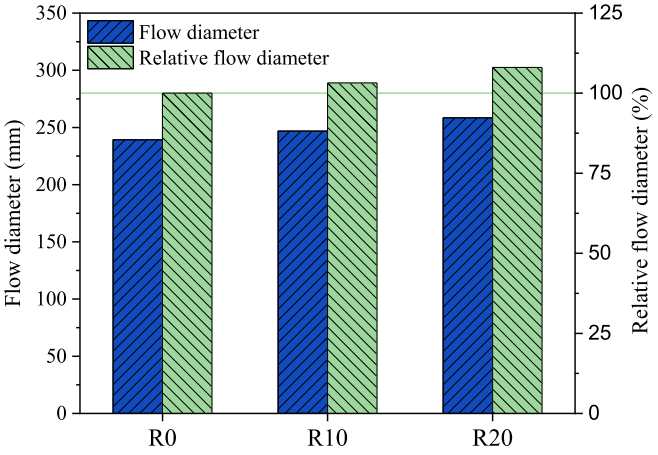

Fig. 3. Flow diameter and Relative flow diameter of the paste.

3. Results and analysis

3.1. Workability

The workability of the LC^3 slurry was characterized using the flow diameter. The flow diameter increases as the amount of RGP increases, as shown in Fig. 3. Compared to R0, the relative flow diameters of R10 and R20 increased by 3.18 % and 8.02 %, respectively. The fluidity can be optimized by considering the physical characteristics of RGP. Firstly, the smooth surface of RGP dispersed in the slurry can promote movement by reducing the friction between particles. Secondly, the low water absorption of RGP can reduce the water required to lubricate its surface, and the released water helps increase the thickness of the water film around the gelled particles [21]. Therefore, the rheological properties and workability of LC^3 can be optimized.

3.2. Hydration heat

Fig. 4 shows the release of hydration heat normalized by the mass of the binder and LC^3. There are four distinct exothermic peaks in the hydration heat curve. Peak I is usually considered to be the rapid dissolution exotherm of the clinker after contact with water [9]. Peak II appeared at approximately 6 h, corresponding to the hydration of the silicate phase in the clinker [8]. Peak III is attributed to renewed dissolution of aluminate and accelerated precipitation of ettringite. Finally, a broad and somewhat indistinct peak, associated with the formation of carboaluminate [22], appeared at approximately 48–60 h.

When the hydration heat is normalized by mass per g binder (Fig. 4 (a)), the II, III, and IV peaks decrease with an increase in the RGP substitution level. First, this is due to the lower pozzolanic activity of RGP in the early stage. Second, the dissolution of silicate phase in clinker is the primary source of heat flow [23]. The decrease of clinker can explain the reduction in heat flow at the peak at the end of the dissolution of the silicate phase. Additionally, added RGP produced a dilution effect, and the filler effect (nucleation sites) of limestone was crippled. Therefore, the main reason for the heat flow reduction is the dilution of the LC^3 gelling material, which is consistent with previous research results [24].

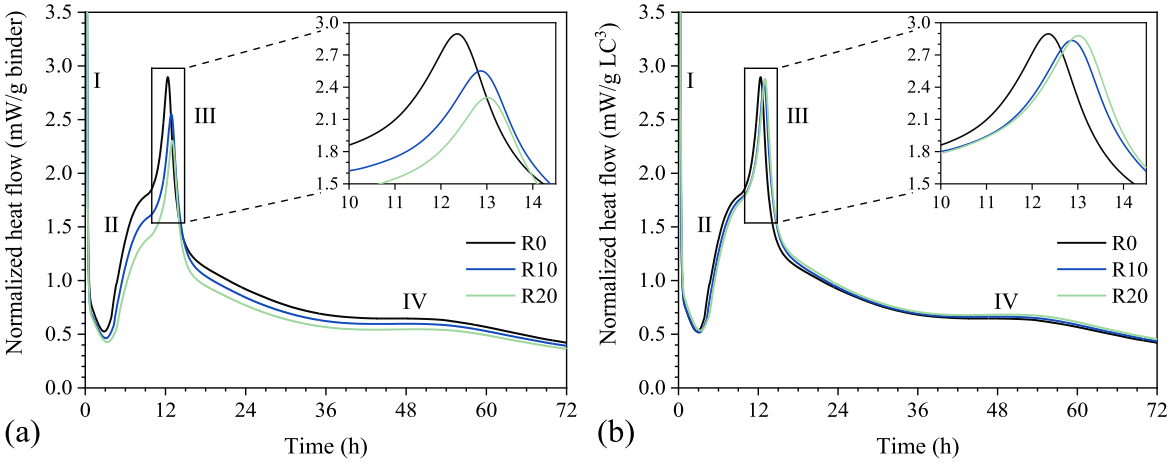

Fig. 4. (a) Heat flow curve and (b) Normalized to LC^3 mass.

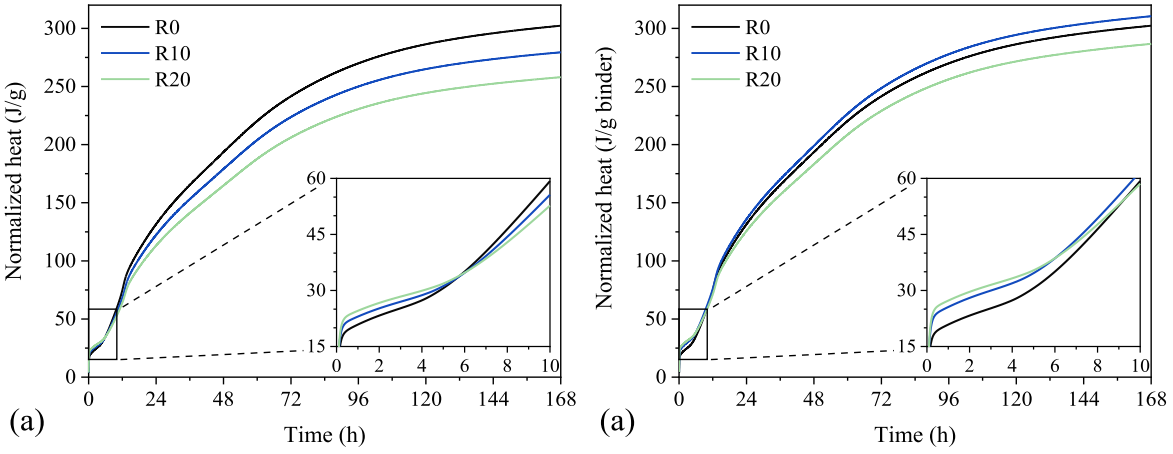

Fig. 5. (a) Cumulative heat flow and (b) Normalized to LC^3 mass.

In addition, Fig. 4 shows that RGP slightly delays hydration by almost 1 h. Liu et al. [25] studied the effects of cleaned and unwashed glass powder on OPC hydration. They claim that unwashed glass powder can cause delayed hydration due to organic contaminants such as sugar. In addition, limestone in LC^3 can accelerate the hydration of the system by providing nucleation sites for CSH [7]. As the RGP substitution level increases, the limestone content decreases, and the nucleation is weakened, resulting in delayed LC^3 hydration.

Fig. 5 shows the cumulative heat normalized by the masses of the binder and LC^3. Fig. 5(a) shows that the cumulative heat release in the first 6 h increased with an increase in the RGP substitution level, which was caused by the exothermic RGP dissolution in the initial stage after stirring. Subsequently, the cumulative heat decreased with a reduced substitution rate, leading to an interesting crossover effect between the curves. The intersection point was located at approximately 6 h, which corresponds to the appearance of peak II in Fig. 4. Combined with the

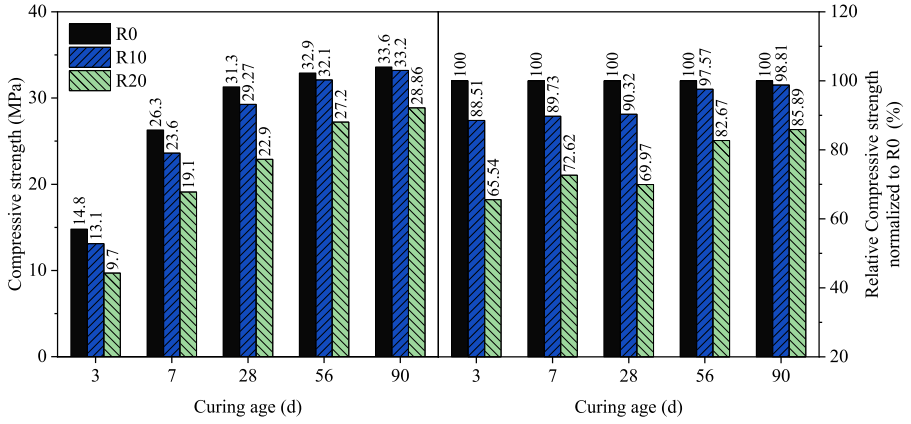

Fig. 6. (a) Compressive strength and (b) Relative Compressive strength for 3, 7, 28, 56, and 90 d.

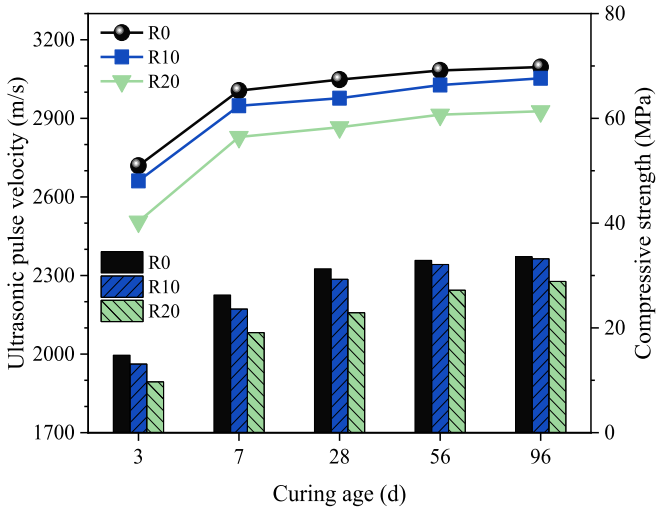

Fig. 7. UPV of the hardened cement paste for 3, 7, 28, 56, and 90 d.

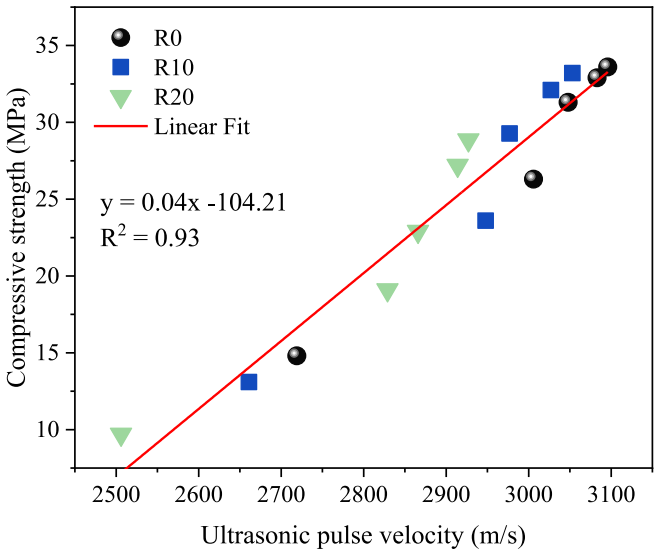

Fig. 8. Relationship between compressive strength and UPV.

decreased intensity of peaks II and III, the decrease in cumulative heat can be attributed to the reduction in hydration owing to the decline in clinker and metakaolin.

For R0, R10, and R20, the LC^3 content was 100 %, 90 %, and 80 %, respectively. When normalized by the mass per gram of LC^3, the cumulative heat increased with increasing RGP content, as shown in Fig. 5 (b). Compared with previous studies, it was found that adding glass powder to LC^3 and OPC both increased the normalized cumulative heat [26]. In addition to the exothermic phenomenon of RGP dissolution in the initial stage, some studies have suggested that an increase in the sodium concentration caused by RGP dissolution can increase the alkalinity of the pore solution, thereby promoting the dissolution and exotherm of clinker [26,27]. In summary, as shown in Fig. 5(a), the negative correlation between the 168 h cumulative heat of LC^3 and the substitution rate is due to the dilution effect of RGP. In Fig. 5(b), the positive correlation between the normalized cumulative heat and substitution rate is related to RGP dissolution and improved clinker hydration by RGP.

3.3. Compressive strength

Fig. 6(a) summarizes the variation changes in compressive strength during the experiment. The partial replacement of LC^3 with RGP resulted in a decrease in strength, similar to the effect of RGP on OPC [3,28]. Combined with the results of the reduction in the cumulative heat (Fig. 4 (a)), it can be speculated that the main reason for the difference in strength between the control group and RGP-LC^3 is the reduction of components, such as clinker and metakaolin. The early activity of RGP was relatively low, whereas the clinker and activated alumina in metakaolin contributed more to the early strength of LC^3. Additionally, a previous study explained that adding RGP to the mixture exerted a dilution effect [26], implying that the effective water-cement ratio increased. A higher water-cement ratio increases the distance between the cement particles in fresh cement slurries, which increases the volume and size of the capillary pores created during hydration [29].

Owing to the low activity of RGP in the early stages and the dilution effect, the early strength growth of RGP-LC^3 was slow. The pozzolanic reaction of RGP mainly occurs at a later age, which can significantly enhance the later strength growth. Fig. 6(b) shows that the relative strength growth of R10 and R20 was only 1.81 % and 4.43 %, respectively, after curing for 3–28 d. During curing from 28 to 56 d, the relative strengths of R10 and R20 increased by 7.25 % and 12.7 %, respectively. Notably, when the curing age is extended to 90 d, the strength of R10 is equivalent to that of R0, which is attributed to the slow volcanic reaction of the RGP with the strength increase in the later stage [3]. However, the relative strength of R20 was the lowest at 90 d. This could be related to the content of calcium hydroxide (CH) as well as the reductions in clinker and metakaolin. Reducing the clinker content leads to decreased CH produced by hydration, whereas the pozzolanic reactions of metakaolin and RGP rely on CH activation. Considering the strong competition of metakaolin with higher and faster pozzolanic activity for CH, this may lead to insufficient CH for activating RGP to generate the C(A)SH gel in the later stage.

3.4. UPV

Fig. 7 summarizes the changes in UPV of the cured slurries during the experiment. As the development of the hydration reaction progresses, hydration products precipitate in the porous cement matrix, and the UPV increases with curing time. However, the UPV decreased with an increase in the RGP substitution level due to the dilution effect resulting from the partial replacement of LC^3 with RGP, which reduced the formation of solid hydration products [30]. The addition of RGP resulted in a decrease in the UPV and strength of the mixture, and the two developmental trends were similar. In this study, UPV can be mutually verified with compressive strength to confirm the reliability of the test. Fig. 8 shows the relationship between the test values obtained in the experiment. A correlation between UPV and strength was obtained by linear regression with an R^2 value of 0.93. This indicates that the UPV of the mixture with the addition of RGP is highly correlated with the strength development.

3.5. XRD

Fig. 9 shows the results of the crystalline phase characterization in the LC^3 hydration product after curing for 3 and 90 d. The typical cement hydration products, such as ettringite (AFt) and CH, can be detected. Monocarbonate (Mc) and hemicarbonate (Hc) were produced under the synergy of metakaolin and limestone, and quartz from metakaolin and calcium carbonate from limestone were detected.

At day 3, the peak intensities of AFt, CH, and MC decreased slightly with a decrease in the clinker phase, metakaolin, and limestone content. Carbonoaluminate reduction may also lead to decreases in strength. Previous studies have shown that Hc and Mc can refine pores, reduce the diffusion coefficient of chloride ions, and improve the strength of the mixture [31,32]. At 90 d, the CH diffraction peaks were difficult to identify owing to the large consumption of metakaolin and the RGP

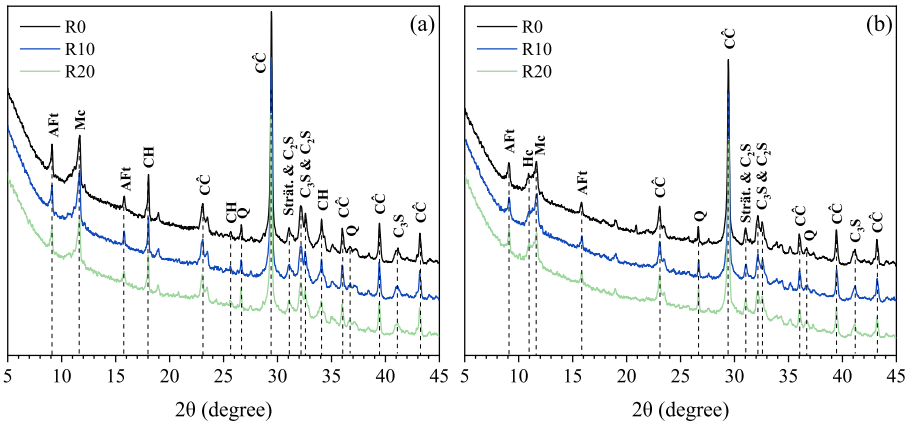

Fig. 9. XRD patterns of the hardened LC^3 paste for 3 d (a) and 90 d (b). AFt = Ettringite, Hc = Hemicarbonate, Mc = Monocarbonate, Q = Quartz, CH = Calcium hydroxide, Strät. = Strätlingite, and CĈ = Calcium carbonate.

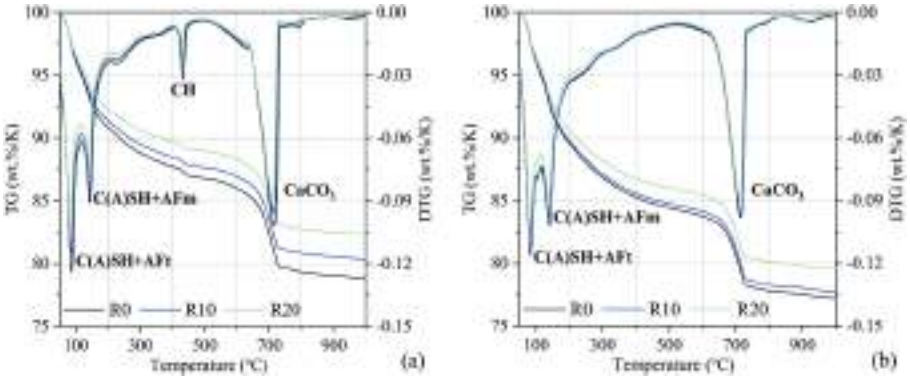

Fig. 10. TG-DTG curves of hardened LC^3 paste for 3 d (a) and 90 d (b).

pozzolanic reaction. This is consistent with the results observed in the study by Krishnan et al. [33]. However, as reported in the study [26], when RGP is incorporated into OPC, a large amount of CH still exists even if it is hydrated for 300 d. Differences in CH content may result in different degrees of pozzolanic reaction of RPG in LC^3 and OPC systems. The decrease in AFt and calcium carbonate peaks were attributed to Hc formation. At the same time, the Mc diffraction peak decreased, indicating that when the CH available for the reaction is insufficient, Mc and Hc can also be consumed to provide Ca^{2+} to form strätlingite [34].

3.6. TG-DTG

TG and DTG curves were used to study the relationship between the mass loss of LC^3 paste and temperature. The DTG curve was obtained from the first derivative of the TG curve with respect to temperature, and the results are shown in Fig. 10. Initially, the free water in the cement paste was released as the temperature increases, before reaching 105 °C. C(A)SH loses interlayer water in a wide temperature range, primarily between 50 and 200 °C. The water molecules contained in AFt were released at approximately 130 °C [35]. The DTG peak generated by the dehydration of the AFm phase can be observed at approximately 170 °C. As the temperature continued to increase, weight loss due to the decomposition of CH to calcium oxide and the release of water vapor was monitored between 400 and 500 °C. When the temperature reaches 620–800 °C, the calcium carbonate in the limestone decomposes into calcium oxide, resulting in the release of CO_2 [36].

At day 3, the amount of generated hydration products, such as CH, decreased sequentially with an increase in the substitution level of clinker, metakaolin, and limestone, primarily due to the dilution effect of RGP. At 90 d, the loss on ignition of C(A)SH + AFt in R0 and R10 was

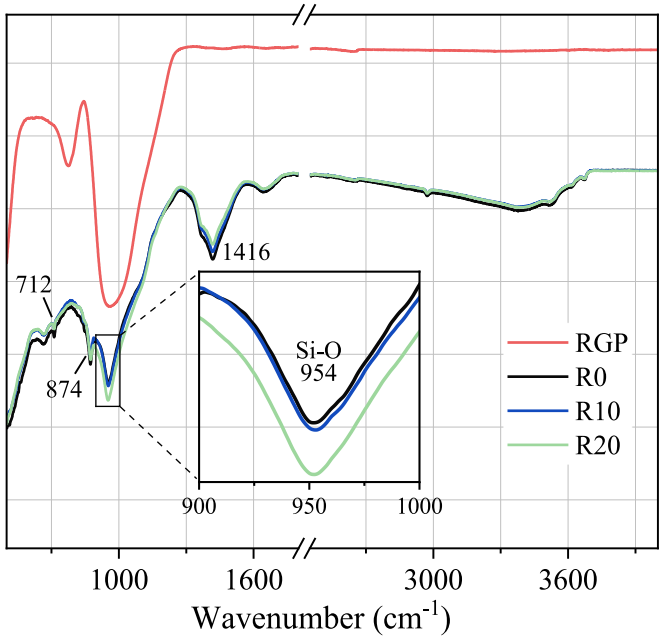

Fig. 11. The change of functional group absorption peak of hardened LC^3 paste in 500–4000 cm^{-1} band.

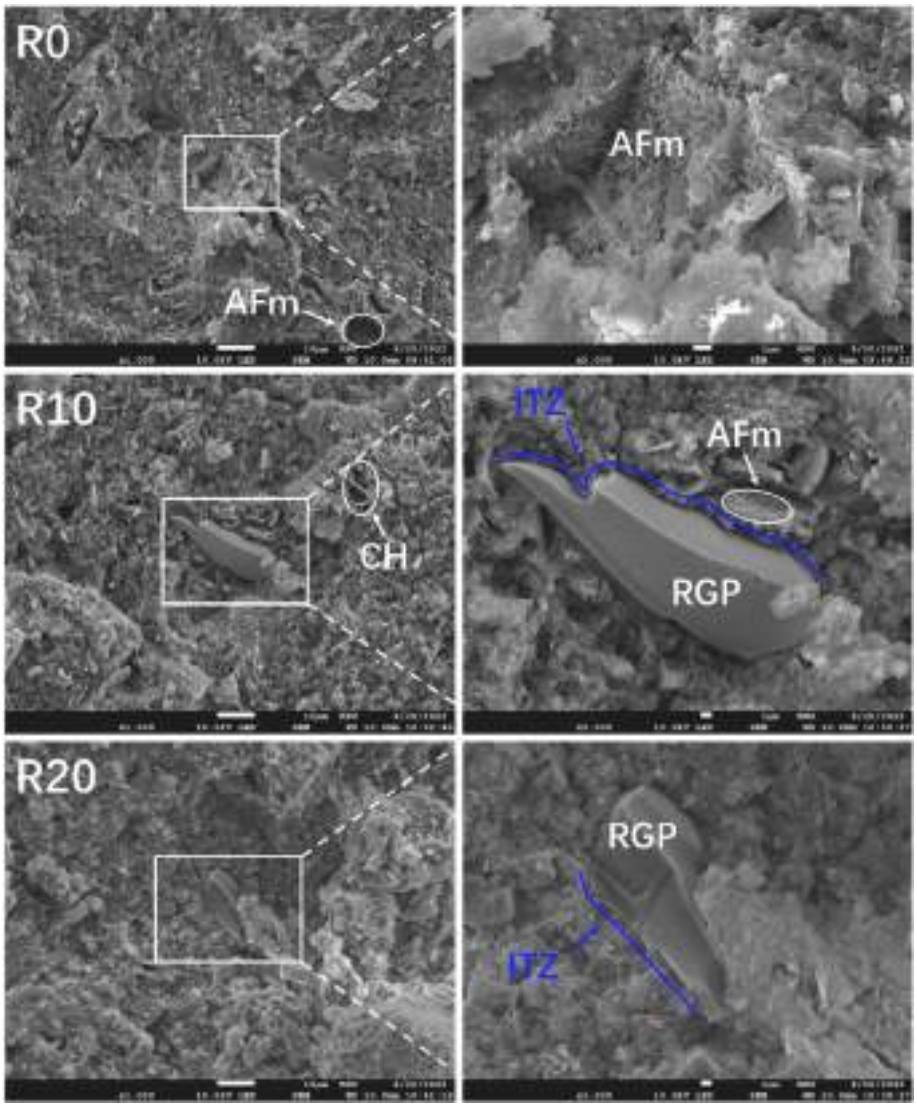

Fig. 12. SEM of hardened LC^3 paste for 90 d.

similar and greater than that of R20. This is consistent with the results of the compressive strength tests. It can be inferred that the pozzolanic reaction of the RGP contributed to the increase in the C(A) SH content in R10. Mejdi et al. [26] reached the same conclusion in their study of glass powder replacing OPC. However, the pozzolanic reaction in R20 failed to significantly increase the C(A) SH content, and the fundamental reason may be that the RGP was not thoroughly activated owing to the lack of CH. The pozzolanic reaction of metakaolin and RGP made the CH in the paste almost completely consumed at 90 d. The TG results confirmed our hypothesis regarding the influence of the CH content on late strength development with the lowest CH generation and highest SCM content of R20 leading to difficulties in late strength improvement.

3.7. FT-IR

Fig. 11 shows the absorption bands of the functional groups in the original RGP and LC^3 hydration products detected using the FT-IR analyzer at 90 d. Pristine RGP exhibits main absorption bands for Si–O bonds and Si–O–Si at 770 cm^{-1} and 890–1090 cm^{-1}, respectively [37]. The absorption band derived from the asymmetric stretching of the Si–O bond in C(A)SH in the hydration product of R0 is located at approximately 951 cm^{-1} [38]. With the incorporation of RGP, the positions of the Si–O bonds remained fixed and their intensity increased, consistent with the results observed by Gao et al. [39]. This indicates that RGP can increase the total number of *Si*–O bonds in the product, but the structural change in the *Si*–O bonds is not apparent. The out-of-plane bending vibration of CO_3^{2-} in limestone causes sharp signals at 874 cm^{-1} and 712 cm^{-1}. The absorption band at 1416 cm^{-1} corresponds to the asymmetric stretching vibration of the O–C–O bond of the CO_3^{2-} group [40]. The signal for CO_3^{2-} decreases with increasing RGP dosage.

3.8. SEM-EDS

Fig. 12 shows the microstructure of the hardened LC^3 paste after curing for 90 d. The presence of the AFm phase in the matrix was observed in the microscopic image of R0. Residual hexagonal sheet-like CH and dehydrated RGP particles encapsulated in the matrix are also observed in R10 and R20. It can be observed that there is a narrow ITZ between the RGP particles and the cement matrix, which may be related to the smooth surface of the RGP. A narrow ITZ leads to a decrease in the mechanical interlock between the cement matrix and the RGP [41], which is one of the reasons for the reduced mechanical properties of the mixture.

EDS technology can be used to determine the elemental composition of the samples. Based on the microscopic appearance of the observation position and the assistance of EDS, the area of the hydration product was

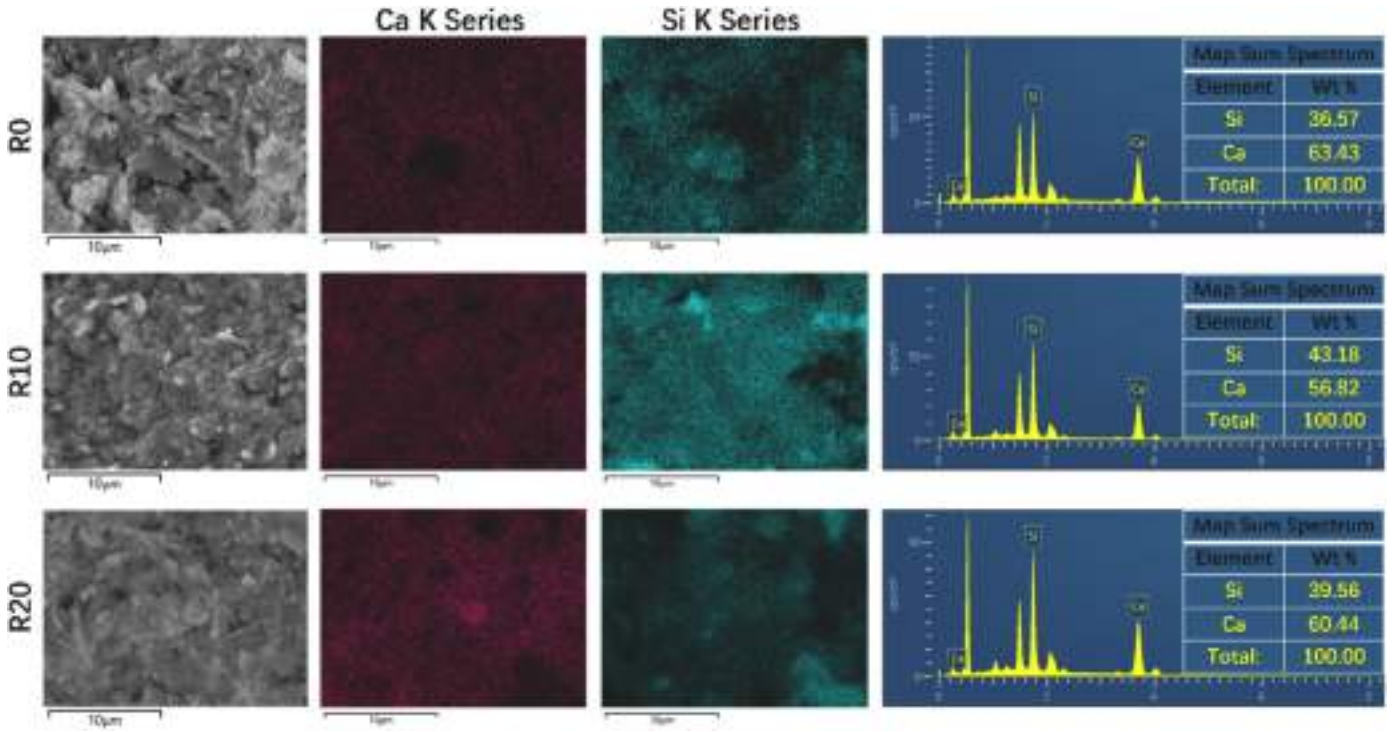

Fig. 13. SEM-EDS of paste for 90 d.

selected for elemental analysis. The mapping analysis of Ca and Si in the hydration products obtained by EDS is shown in Fig. 13. SCM materials typically have a high silica content, and the hydrated calcium silicate gel produced by the pozzolanic reaction has a high Si content and low Ca content [42]. Elemental analysis revealed that the reaction of RGP led to an increase in the total proportion of Si and a decrease in the Ca ratio in R10 and R20. In contrast, the higher proportion of Si in R10 indicates that the pozzolanic activity in R10 was more completely activated to generate a C(A) SH gel [40]. However, because of the low CH content, most of the RGP in R20 was not activated in the pozzolanic reaction, which is consistent with the previous TG analysis results.

4. Discussion

4.1. Effect of RGP on LC^3 performance

The smooth surface and low water absorption of RGP can facilitate particle flow and increase the workability of the LC^3. The slower increase in the early strength of RGP-LC^3 was due to the lower early activity of RGP and the dilution effect. The test confirmed that the compressive strength of RGP-LC^3 with a replacement amount of 10 % was similar to that of the control sample at 90 d. Previous research [26] reported that the hydration of the OPC system produces an amount of CH, which can be used for the pozzolanic reaction of RGP. As the curing time increases, the pozzolanic reaction can increase the strength of OPC in the later stage [43]. Unlike OPC systems, the CH content in LC^3 is low. Considering the competition between metakaolin with high pozzolanic activity and RGP for CH, there may not be sufficient CH for RGP to be consumed in the later stage. Therefore, considering the mechanical properties of building materials, when the substitution amount of RGP in LC^3 is maintained below 10 %, a mixture with similar mechanical properties and higher workability can be obtained.

4.2. Sustainability

4.2.1. Carbon emission assessment

The increase in CO_2 emissions is one of the leading causes of climate change. The production of cement clinker is a high energy- and carbon-intensive process. The LC^3 design significantly reduces the use of the clinker phase and has the potential for rapid market integration. However, metakaolin, which is one of the LC^3 materials, needs to be obtained by calcination of kaolin at 750 °C. This process leads to fuel consumption and greenhouse gas emissions. Performing the deep decarburization of LC^3 on an existing basis is necessary. The RGP exhibited pozzolanic activity and has a low-carbon footprint. Using it as a partial replacement for LC^3 is an effective way to reduce cement CO_2 emissions further and improve environmental benefits.

Table 3
Mixture proportions of paste (kg/m^3).

Mix	Unit Mass				
	OPC	LS	MK	RGP	Water
R0	580.13	158.22	316.43	0.00	632.87
R10	519.45	141.67	283.33	104.94	629.63
R20	459.38	125.28	250.57	208.81	626.42

According to a previous study [44], CO_2 emissions from concrete consist primarily of materials, material transportation, and concrete production. In the actual production process, the CO_2 emissions caused by the transportation and production processes of the material are insignificant compared to the material itself. Therefore, this study focused on CO_2 emissions generated by the materials themselves. Equation (1) was used to calculate the CO_2 emissions of RGP-LC^3 [44].

$$mCO_2 = \sum_{i+1}^{n} (CO_{2i} \times M_i) \quad (1)$$

where mCO_2 represents the CO_2 emission per 1 m^3 of concrete (kg·CO_2/m^3); CO_{2i} represents the CO_2 emission coefficient of various materials. The CO_2 emission factors of OPC, LS, MK, and RGP are 0.863, 0.008, 0.33 [45,46], and 0.02 [24,47,48] respectively, and M_i represents the mass of the various materials per unit volume (kg/m^3), which can be calculated using Equation (2), where ρ_i is the material density. The masses of the materials per unit volume are listed in Table 3.

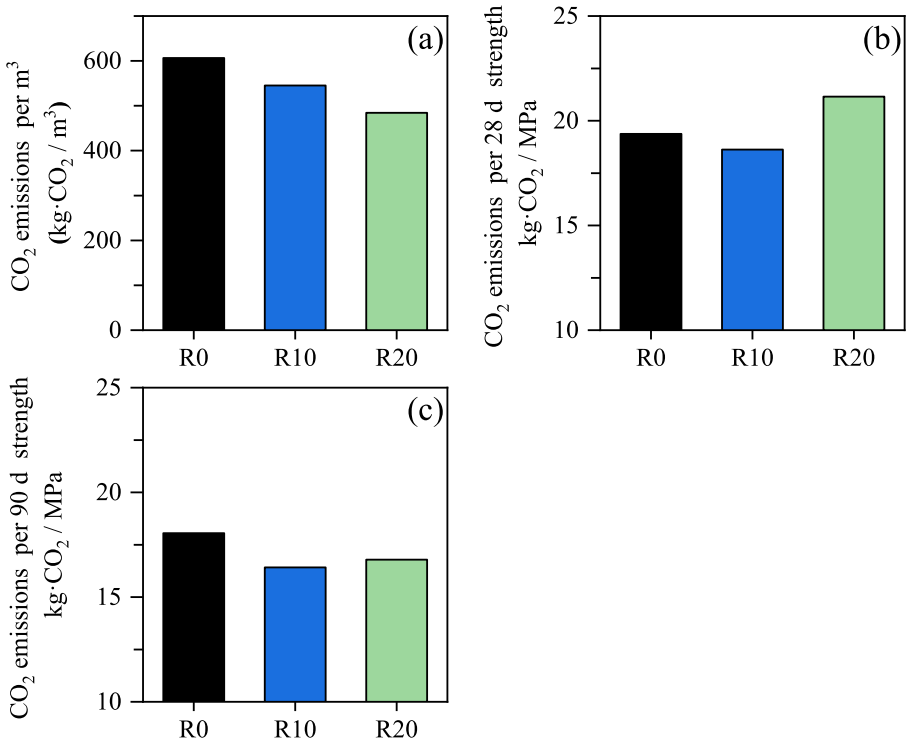

Fig. 14. (A) CO_2 emissions per 1 m^3, (b) per 28 d strength, and (c) per 90 d strength.

$$\sum_{i=1}^{4}\frac{M_i}{\rho_i}=1 \tag{2}$$

In addition, when using alternative materials to reduce CO_2 emissions, considering CO_2 emissions per unit strength is necessary. The CO_2 emissions were normalized according to the 28 and 90 d compressive strengths using Equations (3) and (4).

$$mCO_{2-SC}=\frac{mCO_2}{SC_{28}} \tag{3}$$

$$mCO_{2-SC}=\frac{mCO_2}{SC_{90}} \tag{4}$$

where $mCO_{2\text{-}SC}$ represents the CO_2 emission per unit compressive strength (kg CO_2/MPa); and SC_{28} and SC_{90} represent the compressive strengths of LC^3 after cured for 28 d and 90 d, respectively. A summary of the analysis results is shown in Fig. 14.

Firstly, Fig. 14(a) shows that the CO_2 emissions per cubic meter of LC^3 decreased as the substitution rate of RGP increased. Secondly, when evaluating at 28 d, the CO_2 emissions of R0, R10, and R20 were 19.38, 18.62, and 21.15 $kg{\cdot}CO_2$/MPa, respectively. R10 had the lowest emissions, whereas R20 had the highest, as shown in Fig. 14(b).

Despite having the lowest CO_2 emissions per cubic meter R20 was unable to assist LC^3 achieve emission reduction at 28 d considering the strength. This was due to the dilution effect and the reduction of clinker and metakaolin, which caused the loss of 28 d strength. Finally, when evaluating at 90 d, as shown in Fig. 14(c), the CO_2 emissions per unit strength of R10 were further reduced to 16.42 $kg{\cdot}CO_2$/MPa. Notably, at 90 d, R20 CO_2 emissions reduced to 16.79 $kg{\cdot}CO_2$/MPa, which was lower than R0, 18.05 $kg{\cdot}CO_2$/MPa. The significant difference in the CO_2 emissions of R20 between 28 and 90 d was attributed to the contribution of the slow volcanic reaction of the RGP to the later strength. Referring to the later strength development and XRD and TG analyses of the hydration products, the RGP could not be fully activated owing to insufficient CH and clinker reduction. Consequently, the final strength of R20 was much lower than that of R10; therefore, the emission reduction effect was slightly lower than that of R10. The analysis confirmed the positive emission reduction benefits of RGP. The effective addition of RGP could further reduce CO_2 emissions while ensuring the performance of LC^3.

The use of building materials is a long-term process. When evaluating the CO_2 emission per unit strength of materials, most experimental studies only consider the 28 d compressive strength. This method may result in the contribution of pozzolanic materials to the later strength and CO_2 emission reduction being ignored. Therefore, the age of evaluation needs to be carefully selected. From the analysis in this study, future work is recommended to include a more reasonable evaluation of the 90 d compressive strength when the mixture slowly incorporates pozzolanic reactive materials such as RGP.

4.2.2. *Improvements to landfill*

Approximately 130 million tons of waste glass are produced annually, 75 % of which is in landfills. Every ton of waste glass landfilled occupies approximately 1.5 cubic meters of space [49]. Currently, the available land area is limited, and traditional landfill methods have exacerbated the land crisis. The environmental hazards of expanding landfills to the surrounding areas include the generation of highly polluted and toxic leachate, the subsequent disposal of which is challenging. Moreover, when leachate leaks, the pollution of groundwater and the soil environment is devastating. In addition, the hazardous gases produced during the waste degradation process severely affect the quality of life of the surrounding residents.

Society is moving towards green sustainability, and the sustainable management of solid waste is an area of continuous research. Owing to the high demand for building materials in the construction industry, using waste glass as a building material is a suitable option for its quick disposal. Recycled materials are more competitive in regions where SCM and landfills have limited availability. For example, the method proposed in this study uses RGP as a partial replacement for LC^3. This approach can potentially lead to a significant consumption of waste

glass in various regions, especially as LC^3 gradually gains market share in the cement industry.

5. Conclusion

This study investigated and evaluated the effects of RGP as an alternative to SCM on LC^3. The hydration, mechanical properties, product composition, and microstructure of LC^3 were comprehensively analyzed at RGP substitution levels of 0, 10, and 20 %, and the sustainability of the approach was assessed. The conclusions of the study are summarized below.

(1) RGP helped improve the workability of LC^3 and substitutions of 10 and 20 % increase the flow diameter by 3.18 % and 8.02 %, respectively. The 90 d compressive strength at a 10 % substitution level was similar to that of the control sample. A further increase of 20 % was detrimental to strength.
(2) With an increase in the substitution level, the hydration heat increased in the early stage and decreased in the later stage. The cumulative heat curve showed a cross effect at approximately 6 h. Owing to the reduction in the clinker and metakaolin, the 10 and 20 % substitutions reduced the cumulative heat reduction of the mixture for 168 h to 7.57 % and 14.65 %, respectively.
(3) The content of the hydration products (C(A) SH + AFt) decreased with increasing substitution amounts at 3 d. The content of hydration products in the mixture containing 10 % RGP at 90 d was the same as that in the control samples, as determined by TG analysis. EDX analysis showed that the proportion of Si in the hydration products increased, whereas that of Ca decreased.
(4) CO_2 emissions per 1 m^3 decreased from 606.46 $kg{\cdot}CO_2/m^3$ to 545.14 and 484.43 $kg{\cdot}CO_2/m^3$ with an increase in substitution rate. The 10 % substitution resulted in the lowest CO_2 emissions per MPa at 28 and 90 d. To avoid ignoring the contribution of the pozzolanic reaction, the 90 d strength should be used as the standard when evaluating the CO_2 emissions of cement containing SCM in future studies.
(5) Considering various factors, such as strength development, workability, and CO_2 emissions, a 10 % substitution rate of RGP in LC^3 is the optimal choice. At this substitution level, the mixture showed similar strength to the control sample, but with higher workability, lower heat of hydration, and lower carbon footprint.

CRediT authors statement

Yi-Sheng Wang: Methodology, Data curation, Formal analysis, Investigation, Writing – original draft. Seokhoon Oh**:** Funding acquisition, Conceptualization, Supervision. **Shafiq Ishak:** Data curation, Investigation, Validation. **Xiao-Yong Wang:** Funding acquisition, Conceptualization, Supervision, Methodology, Writing – review & editing. **Seungmin Lim:** Supervision, Methodology, Writing – review & editing.

Declaration of competing interest

The authors declare the following financial interests/personal relationships which may be considered as potential competing interests: Xiao-Yong Wang reports financial support was provided by National Research Foundation of Korea. Seokhoon Oh reports financial support was provided by Nuclear Safety Research Program through the Korea Foundation of Nuclear Safety.

Acknowledgments

This research was supported by the National Research Foundation of Korea (NRF) grant funded by the Korean Government (MSIT) (No. RS-2023-00208720). Yi-Sheng Wang thanks the China Scholarship Council (CSC) for the financial support (No. 202308260012). This work was supported by the Nuclear Safety Research Program through the Korea Foundation of Nuclear Safety (KoFONS), using financial resources granted by the Nuclear Safety and Security Commission (NSSC) of the Republic of Korea (No. 1075001384).

References

[1] Dadsetan S, Siad H, Lachemi M, Mahmoodi O, Sahmaran M. Optimization and characterization of geopolymer binders from ceramic waste, glass waste and sodium glass liquid. J Clean Prod 2022;342:130931.
[2] Carsana M, Frassoni M, Bertolini L. Comparison of ground waste glass with other supplementary cementitious materials. Cement Concr Compos 2014;45:39–45.
[3] Islam GS, Rahman M, Kazi N. Waste glass powder as partial replacement of cement for sustainable concrete practice. Int J Sustainable Built Environ 2017;6(1):37–44.
[4] Du H, Tan KH. Properties of high volume glass powder concrete. Cement Concr Compos 2017;75:22–9.
[5] Peng L, Zhao Y, Ban J, Wang Y, Shen P, Lu J-X, et al. Enhancing the corrosion resistance of recycled aggregate concrete by incorporating waste glass powder. Cement Concr Compos 2023;137:104909.
[6] Zhan P-m, Zhang X-x, He Z-h, Shi J-y, Gencel O, Yen NTH, et al. Strength, microstructure and nanomechanical properties of recycled aggregate concrete containing waste glass powder and steel slag powder. J Clean Prod 2022;341:130892.
[7] Zunino F, Scrivener K. The reaction between metakaolin and limestone and its effect in porosity refinement and mechanical properties. Cement Concr Res 2021;140:106307.
[8] Scrivener K, Martirena F, Bishnoi S, Maity S. Calcined clay limestone cements (LC3). Cement Concr Res 2018;114:49–56.
[9] Sharma M, Bishnoi S, Martirena F, Scrivener K. Limestone calcined clay cement and concrete: a state-of-the-art review. Cement Concr Res 2021;149:106564.
[10] Scrivener K, Avet F, Maraghechi H, Zunino F, Ston J, Hanpongpun W, et al. Impacting factors and properties of limestone calcined clay cements (LC3). Green Mater 2018;7(1):3–14.
[11] Al-Fakih A, Al-Awsh W, Al-Koshab MQA, Al-Shugaa MA, Al-Osta MA, Drmosh Q, et al. Effects of zeolitic imidazolate framework-8 nanoparticles on physicomechanical properties and microstructure of limestone calcined clay cement mortar. Construct Build Mater 2023;366:130236.
[12] Long W-J, Wu Z, Khayat KH, Wei J, Dong B, Xing F, et al. Design, dynamic performance and ecological efficiency of fiber-reinforced mortars with different binder systems: ordinary Portland cement, limestone calcined clay cement and alkali-activated slag. J Clean Prod 2022;337:130478.
[13] Zhang M, Yang L, Wang F. Understanding the longer-term effects of C–S–H seeding materials on the performance of limestone calcined clay cement. Construct Build Mater 2023;392:131829.
[14] Andrew RM. Global CO 2 emissions from cement production. Earth Syst Sci Data 2018;10(1):195–217.
[15] Elaqra HA, Abou Haloub MA, Rustom RN. Effect of new mixing method of glass powder as cement replacement on mechanical behavior of concrete. Construct Build Mater 2019;203:75–82.
[16] Fanijo EO, Kassem E, Ibrahim A. ASR mitigation using binary and ternary blends with waste glass powder. Construct Build Mater 2021;280:122425.
[17] Matos AM, Sousa-Coutinho J. Durability of mortar using waste glass powder as cement replacement. Construct Build Mater 2012;36:205–15.
[18] Bostanci SC. Use of waste marble dust and recycled glass for sustainable concrete production. J Clean Prod 2020;251:119785.
[19] Zhang T, Lu Z, Sun Z, Yang H, Yan Z, Ji Y. Modification of glass powder and its effect on the compressive strength of hardened alkali-activated slag-glass powder paste. J Build Eng 2022;58:105030.
[20] Wang Y-S, Tae S-H, Lin R-S, Wang X-Y. Effects of Na2CO3 on engineering properties of cement–limestone powder–slag ternary blends. J Build Eng 2022;57:104937.
[21] Lu J-x, Duan Z-h, Poon CS. Combined use of waste glass powder and cullet in architectural mortar. Cement Concr Compos 2017;82:34–44.
[22] Parashar A, Bishnoi S. Hydration behaviour of limestone-calcined clay and limestone-slag blends in ternary cement. RILEM Technical Letters 2021;6:17–24.
[23] Pane I, Hansen W. Investigation of blended cement hydration by isothermal calorimetry and thermal analysis. Cement Concr Res 2005;35(6):1155–64.
[24] Soliman N, Tagnit-Hamou A. Development of ultra-high-performance concrete using glass powder–Towards ecofriendly concrete. Construct Build Mater 2016;125:600–12.
[25] Liu G, Florea M, Brouwers H. The hydration and microstructure characteristics of cement pastes with high volume organic-contaminated waste glass powder. Construct Build Mater 2018;187:1177–89.
[26] Mejdi M, Wilson W, Saillio M, Chaussadent T, Divet L, Tagnit-Hamou A. Hydration and microstructure of glass powder cement pastes–A multi-technique investigation. Cement Concr Res 2022;151:106610.
[27] Zheng K. Pozzolanic reaction of glass powder and its role in controlling alkali–silica reaction. Cement Concr Compos 2016;67:30–8.
[28] Jiang Y, Ling T-C, Mo KH, Shi C. A critical review of waste glass powder–Multiple roles of utilization in cement-based materials and construction products. J Environ Manag 2019;242:440–9.

[29] Lafhaj Z, Goueygou M, Djerbi A, Kaczmarek M. Correlation between porosity, permeability and ultrasonic parameters of mortar with variable water/cement ratio and water content. Cement Concr Res 2006;36(4):625–33.
[30] Schwarz N, DuBois M, Neithalath N. Electrical conductivity based characterization of plain and coarse glass powder modified cement pastes. Cement Concr Compos 2007;29(9):656–66.
[31] Ramezanianpour AM, Hooton RD. A study on hydration, compressive strength, and porosity of Portland-limestone cement mixes containing SCMs. Cement Concr Compos 2014;51:1–13.
[32] Krishnan S, Bishnoi S. Understanding the hydration of dolomite in cementitious systems with reactive aluminosilicates such as calcined clay. Cement Concr Res 2018;108:116–28.
[33] Krishnan S, Bishnoi S. A numerical approach for designing composite cements with calcined clay and limestone. Cement Concr Res 2020;138:106232.
[34] Zunino F, Scrivener K. Microstructural developments of limestone calcined clay cement (LC3) pastes after long-term (3 years) hydration. Cement Concr Res 2022;153:106693.
[35] Song H, Jeong Y, Bae S, Jun Y, Yoon S, Oh JE. A study of thermal decomposition of phases in cementitious systems using HT-XRD and TG. Construct Build Mater 2018;169:648–61.
[36] Chan CL, Zhang M. Effect of limestone on engineering properties of alkali-activated concrete: a review. Construct Build Mater 2023;362:129709.
[37] Burciaga-Díaz O, Durón-Sifuentes M, Díaz-Guillén J, Escalante-García J. Effect of waste glass incorporation on the properties of geopolymers formulated with low purity metakaolin. Cement Concr Compos 2020;107:103492.
[38] Yan Y, Yang S-Y, Miron GD, Collings IE, L'Hôpital E, Skibsted J, et al. Effect of alkali hydroxide on calcium silicate hydrate (CSH). Cement Concr Res 2022;151:106636.
[39] Gao X, Yu Q, Li X, Yuan Y. Assessing the modification efficiency of waste glass powder in hydraulic construction materials. Construct Build Mater 2020;263:120111.
[40] Wang Y-S, Wang X-Y. Multi-characterizations of the hydration, microstructure, and mechanical properties of a biochar–limestone calcined clay cement (LC3) mixture. J Mater Res Technol 2023;24:3691–703.
[41] Jiang X, Xiao R, Ma Y, Zhang M, Bai Y, Huang B. Influence of waste glass powder on the physico-mechanical properties and microstructures of fly ash-based geopolymer paste after exposure to high temperatures. Construct Build Mater 2020;262:120579.
[42] Skibsted J, Snellings R. Reactivity of supplementary cementitious materials (SCMs) in cement blends. Cement Concr Res 2019;124:105799.
[43] Kamali M, Ghahremaninezhad A. An investigation into the hydration and microstructure of cement pastes modified with glass powders. Construct Build Mater 2016;112:915–24.
[44] Yang K-H, Jung Y-B, Cho M-S, Tae S-H. Effect of supplementary cementitious materials on reduction of CO2 emissions from concrete. J Clean Prod 2015;103:774–83.
[45] Miller SA, John VM, Pacca SA, Horvath A. Carbon dioxide reduction potential in the global cement industry by 2050. Cement Concr Res 2018;114:115–24.
[46] Xuan M-Y, Wang X-Y. Autogenous shrinkage reduction and strength improvement of ultra-high-strength concrete using belite-rich Portland cement. J Build Eng 2022;59:105107.
[47] Tahwia AM, Essam A, Tayeh BA, Abd Elrahman M. Enhancing sustainability of ultra-high performance concrete utilizing high-volume waste glass powder. Case Stud Constr Mater 2022;17:e01648.
[48] Boden TA, Marland G, Andres RJ. National CO2 emissions from fossil-fuel burning, cement manufacture, and gas flaring: 1751-2014, Carbon Dioxide Information Analysis Center. Oak Ridge National Laboratory, US Department of Energy; 2017.
[49] Ferdous W, Manalo A, Siddique R, Mendis P, Zhuge Y, Wong HS, et al. Recycling of landfill wastes (tyres, plastics and glass) in construction–A review on global waste generation, performance, application and future opportunities. Resour Conserv Recycl 2021;173:105745.